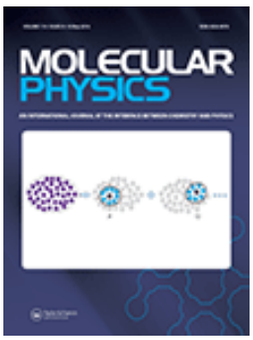

Taylor & Francis
Taylor & Francis Group

Molecular Physics

An International Journal at the Interface Between Chemistry and Physics

ISSN: 0026-8976 (Print) 1362-3028 (Online) Journal homepage: https://www.tandfonline.com/loi/tmph20

Metal–ring interactions in actinide sandwich compounds: A combined normalized elimination of the small component and local vibrational mode study

Małgorzata Z. Makoś, Wenli Zou, Marek Freindorf & Elfi Kraka

To cite this article: Małgorzata Z. Makoś, Wenli Zou, Marek Freindorf & Elfi Kraka (2020): Metal–ring interactions in actinide sandwich compounds: A combined normalized elimination of the small component and local vibrational mode study, Molecular Physics, DOI: 10.1080/00268976.2020.1768314

To link to this article: https://doi.org/10.1080/00268976.2020.1768314

Published online: 21 May 2020.

MOLECULAR PHYSICS e1768314
https://doi.org/10.1080/00268976.2020.1768314

Taylor & Francis
Taylor & Francis Group

SPECIAL ISSUE OF MOLECULAR PHYSICS IN HONOUR OF JüRGEN GAUSS

Metal–ring interactions in actinide sandwich compounds: A combined normalized elimination of the small component and local vibrational mode study

Małgorzata Z. Makoś [a], Wenli Zou [b], Marek Freindorf [a] and Elfi Kraka [a]

[a]Computational and Theoretical Chemistry Group (CATCO), Southern Methodist University, Dallas, TX, USA; [b]Institute of Modern Physics, Northwest University, and Shaanxi Key Laboratory for Theoretical Physics Frontiers, Xi'an, Shaanxi, People's Republic of China

ABSTRACT

The relativistic Hamiltonian Normalised Elimination of the Small Component with atomic unitary transformation (NESCau) was used for the first time to calculate geometries and harmonic vibrational frequencies of actinide sandwich compounds $An(C_nH_n)_2$ (An: Th, Pa, U, Np, Pu; $n = 5-8$). In addition, the Local Vibrational Mode analysis, the Natural Bond Orbital analysis, and the Atoms in Molecules analysis were applied to quantitatively assess the intrinsic strength and the nature of the An-ring interactions. Our results show that actinide sandwich compounds prefer strong covalent interactions between actinide and carbon atoms, similar to those found for homologous ferrocene-type complexes $Fe(C_nH_n)_2$. The metal centre rather than the ring size plays a key role in the strength of those interactions.

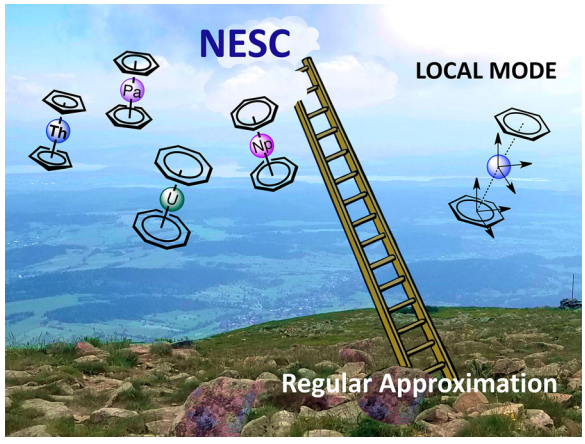

ARTICLE HISTORY
Received 19 March 2020
Accepted 6 May 2020

KEYWORDS
NESCau; actinides; sandwich compounds; local mode analysis; intrinsic bond strength

1. Introduction

The discovery of ferrocene, $Fe(C_5H_5)_2$, in 1951 [1], added a new important field to organometallic chemistry: metal sandwich complexes [2]. The first synthesis of sandwich complexes using an actinide metal centre was reported in 1968 [3] followed by the series $M(C_8H_8)_2$(M = Th, U, Np, Pu) [4,5]. Organometallic complexes of actinide-η^n-carbocyclic derivatives were added to the repertoire because they showed promising magnetic, electronic, photo-physical and catalytic properties [6–9]. The last few years have seen a significant increase of the synthesis of thorium and uranium sandwich complexes [10–14]. In addition, neptunium and plutonium complexes with four (C_5H_5) and two (C_8H_8) ligands have shown a unique behaviour in many small-molecule reactions [15,16]. In order to further develop the field of actinide sandwich complexes, a deeper and more comprehensive understanding of f-block metal-ligand bonding is needed. The experimental investigation of actinide compounds is extremely challenging because of their harmful radioactive character. Also computational studies are difficult, because they require a careful

CONTACT Elfi Kraka ekraka@gmail.com Computational and Theoretical Chemistry Group (CATCO), Southern Methodist University, 3215 Daniel Avenue, Dallas, TX 75275-0314, USA

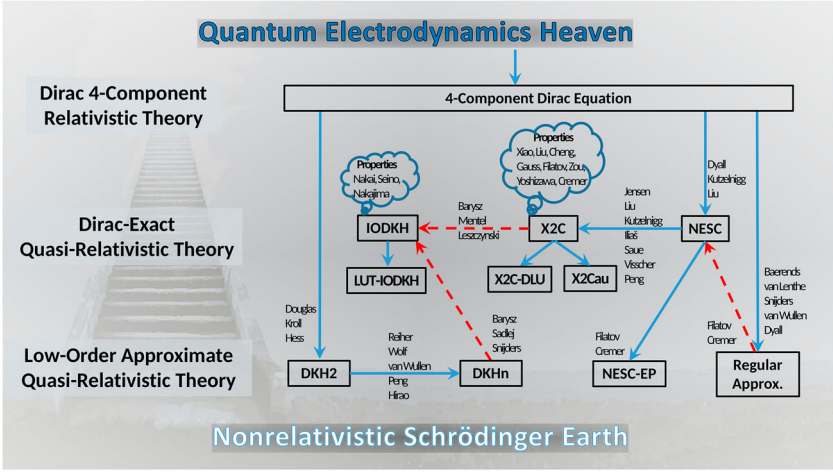

Figure 1. NESC: Normalised Elimination of the Small Component [23,24]; NESC-EP: NESC using an Effective Potential [25]; X2C: eXact Two-Component [27–32]; DKH2: Second-Order Douglas-Kroll-Hess [33,34]; DKHn: *n*th-Order Douglas-Kroll-Hess [35–38]; IODKH: Infinite-Order Douglas-Kroll-Hess [39–41].

consideration of relativistic effects, which play a significant role for the modelling and prediction of reliable physical and chemical properties of compounds with heavy elements, i.e. atoms with an atomic number larger than 20 [17,18], as pointed out in the pioneering work of Desclaux [19], Grant [20] and Pyykkö [21,22]. One has also to consider that relativistic calculations may significantly increase the computational costs; therefore it is imperative to find the right balance between accuracy and efficiency.

Over the past decades a lot of effort has been put into the development of quantum chemical methods including relativistic effects [23–41]. In analogy with Perdew's prominent 'Jacob's ladder' of density functional theory [42] one can establish a relativistic Jacob's ladder, as sketched in Figure 1 stretching from the non-relativistic earth to the quantum electrodynamics (QED) heaven [43,44].

The most rigorous way to include relativity in the calculation of molecular systems is to use Dirac's full 4-component (4c) formalism leading to wave functions being vectors of four complex numbers (known as bispinors) [45,46]. A large variety of approximate methods (the lower ladders in Figure 1) have been derived over the years, motivated by the assumption that the full 4c approach is computationally too demanding and cannot be applied to larger molecules. One of the most popular approximation is the so-called 2-component (2c) approximation, derived from decoupling the large and small components of the Dirac spinor. This approach forms the basis for two important families; the Douglas-Kroll-Hess (DKH) [47,48] method and the regular approximation (RA) [49]. The most famous DKH-type Hamiltonian is the second-order DKH (DKH2) [47,48], which encouraged the development of higher finite-order Hamiltonians, the so-called DKHn Hamiltonians [50–52]. Concerning the RA family, the zeroth-order RA (ZORA) has been widely used in different forms [53,54]. It is important to note that these low-order approximate relativistic Hamiltonians do not treat the core orbitals exactly.

In 1997, Dyall developed the Normalised Elimination of the Small Component (NESC) method [23,24], an important milestone, as NESC could be identified as the first Dirac-exact 2-component relativistic approach (X2C), i.e. a quasi-relativistic (2c) method, which reproduces the one-electron energies of the original 4-component Dirac method and treats both core and valence orbitals exactly [55]. Dyall's work was the starting point for the development of a whole family of X2C relativistic methods [56–61], also called Dirac-exact NESC methods [62–69], defining the upper ladders in Figure 1. Nowadays, X2C methods are the most popular exact relativistic methods for the characterisation of compounds with heavy atoms [26]. Another well-known exact relativistic method is the infinite-order DKH (IODKH; also called infinite-order two-component) method [70,71], which is based on the Barysz-Sadlej-Snijders (BSS) approach [72]. A comprehensive review of those approaches are collected in Ref. [73].

Since the X2C Hamiltonian is mathematically simpler, analytic nuclear gradients [27–29,74] and analytic Hessians [31,32,56] have been derived, being important for relativistic geometry optimisations and frequency calculations. Recently, we adopted a new version of NESC using the atomic approximation (NESCau), which substantially increases the efficiency of relativistic calculations [56], as demonstrated in this work.

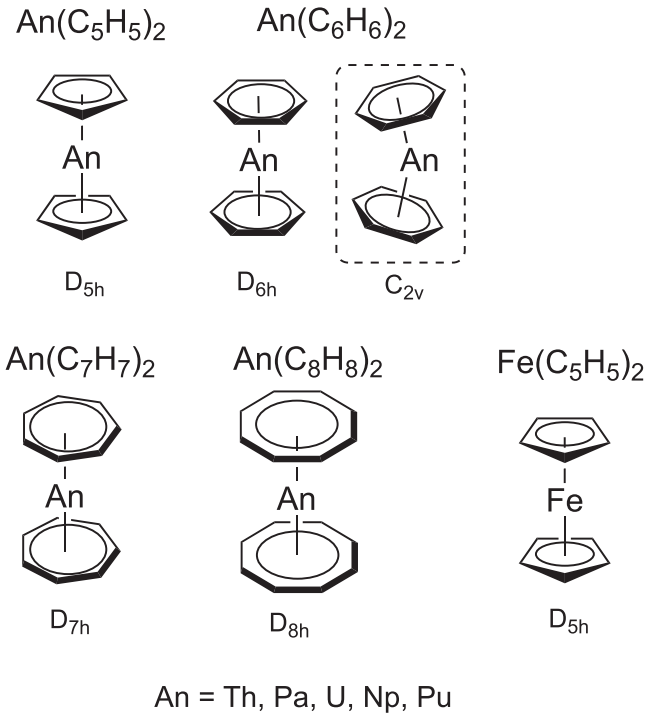

Figure 2. Schematic representation of all complexes investigated in this work. In the case of $An(C_6H_6)_2$ bent structures with C_{2v} symmetry were more stable than the D_{6h} structures.

In addition to choosing the appropriate relativistic method for the description of the actinide sandwich compounds, a suitable measure assessing the intrinsic strength of the An-ring interaction is needed. The local vibrational mode analysis, originally developed by Konkoli and Cremer [75–78] provides the perfect tool for this purpose. So far, the local mode analysis has been successfully applied for the characterisation of covalent bonds [79–85], a broad range of weak chemical interactions in gas phase, solution and an enzyme environment [86–102], as well as chemical bonding in periodic systems and crystals [103,104]. In this work, we extended the local vibrational mode analysis by introducing a new quantitative measure of the intrinsic strength of metal–ring interactions in metal sandwich compounds, as is further described below.

A test set of 20 $An(C_nH_n)_2$ ($n = 5-8$; An = Th, Pa, U, Np, Pu) complexes (see Figure 2) was investigated in this work with NESCau followed by the local mode analysis, in order to deepen our understanding of actinide–ligand bonding, focusing in particular on the following objectives:

- to determine the strength of the An-ring interaction in $An(C_nH_n)_2$ utilising the local mode analysis;
- to investigate how the strength of the An-ring interaction is related to 5f orbital occupation;
- to determine the intrinsic strength of the An-C ring bonds, in particular their covalent or non-covalent character;
- to compare metal–ring interactions of $An(C_nH_n)_2$ with those of the $Fe(C_5H_5)_2$ prototype.

The paper is arranged as follows. In Section 2, we provide details about the computational methods applied including a description of NESCau and the local mode analysis. In Section 3, we systematically elucidate the An-ring interactions and discuss the most important factors determining the stability of these complexes; including local stretching force constants as bond strength descriptors, the natural bond orbital (NBO) analysis [105] exploring 5f occupation, and the topological analysis of the electron density analysing the covalent character of An-ring bonding. The last section summarises the most important results and draws some conclusion which are useful for future fine-tuning and design of actinide sandwich compounds.

2. Computational method

2.1. Normalised elimination of the small component

The continuous development of NESC has been described in several articles [29,32,62–65,67,106,107] including two reviews [26,66], and a number of applications have been reported [27,68,69,108,109]. Therefore, in the following only a short introduction of NESC is given focusing on the NESCau extension.

Starting from the 4c-Dirac equation with embedded restricted kinetic balance (RKB), a Dirac equation in matrix picture was obtained by Dyall [23],

$$\begin{pmatrix} \mathbf{V} & \mathbf{T} \\ \mathbf{T} & \mathbf{W}-\mathbf{T} \end{pmatrix} \begin{pmatrix} \mathbf{A}_- & \mathbf{A}_+ \\ \mathbf{B}_- & \mathbf{B}_+ \end{pmatrix} = \begin{pmatrix} \mathbf{S} & \mathbf{0} \\ \mathbf{0} & \frac{1}{2c^2}\mathbf{T} \end{pmatrix} \begin{pmatrix} \mathbf{A}_- & \mathbf{A}_+ \\ \mathbf{B}_- & \mathbf{B}_+ \end{pmatrix} \begin{pmatrix} \boldsymbol{\varepsilon}_- & \mathbf{0} \\ \mathbf{0} & \boldsymbol{\varepsilon}_+ \end{pmatrix} \quad (1)$$

where **S**, **T** and **V** are, respectively, the overlap, kinetic energy and nuclear attraction integral matrices, **W** is the matrix of the operator $(\boldsymbol{\sigma}\cdot\mathbf{p})V(\mathbf{r})(\boldsymbol{\sigma}\cdot\mathbf{p})/(4c^2)$, and $\boldsymbol{\varepsilon}_+$ ($\boldsymbol{\varepsilon}_-$) is the electronic (positronic) eigenvalues with the eigenvectors $\mathbf{A}_+$ ($\mathbf{A}_-$) for large component and $\mathbf{B}_+$ ($\mathbf{B}_-$) for pseudo-large component. Chemists are generally not interested in the positronic solutions in $\boldsymbol{\varepsilon}_-$, i.e. they are discarded. After some algebra, Dyall derived the NESC equation considering only the electronic eigenvalues $\boldsymbol{\varepsilon}_+$:

$$\tilde{\mathbf{L}}\mathbf{A}_+ = \tilde{\mathbf{S}}\mathbf{A}_+\boldsymbol{\varepsilon}_+ \quad (2)$$

with the NESC Hamiltonian

$$\tilde{\mathbf{L}} = \mathbf{U}^\dagger\mathbf{T} + \mathbf{T}\mathbf{U} - \mathbf{U}^\dagger(\mathbf{T}-\mathbf{W})\mathbf{U} + \mathbf{V} \quad (3)$$

and the metric

$$\tilde{\mathbf{S}} = \mathbf{S} + \frac{1}{2c^2}\mathbf{U}^\dagger\mathbf{T}\mathbf{U}. \tag{4}$$

In above equations, $\mathbf{U}$ can be calculated by $\mathbf{B}_+ = \mathbf{U}\mathbf{A}_+$.

Within the one-electron approximation to the many-body relativistic problem, the NESC Hamiltonian $\tilde{\mathbf{L}}$ has to be renormalised on the non-relativistic metric $\mathbf{S}$ through the following equation

$$\mathbf{H}^{\mathrm{NESC}} = \mathbf{G}^\dagger\tilde{\mathbf{L}}\mathbf{G} \tag{5}$$

where the renormalisation matrix [60] is given by

$$\mathbf{G} = \mathbf{S}^{-1/2}\mathbf{K}\,\mathbf{S}^{1/2}, \tag{6}$$

$$\mathbf{K} = \left(\mathbf{S}^{-1/2}\tilde{\mathbf{S}}\mathbf{S}^{-1/2}\right)^{-1/2}. \tag{7}$$

The renormalised NESC Hamiltonian $\mathbf{H}^{\mathrm{NESC}}$ in Equation (5) is then used to replace the one-electron Hamiltonian in the non-relativistic Fock matrix leading to the coverage of relativistic effects. This is the essence of the Dirac-exact NESC method [106], also called X2C method, as stated [110].

Compared to other relativistic methods, NESC (i.e. X2C) has the advantage of accuracy, simplicity and efficiency [59]. However, for medium-sized and larger molecules, NESC becomes time-consuming due to the involved matrix inversion and diagonalisation procedures. An efficient cure for this problem is the so-called *From Atoms To Molecule* approach [59]. Considering that the molecular $\mathbf{U}$ matrix is substantially atomically local, it can be approximated by the direct sum of a series of atomic $\mathbf{U}$ matrices; similarly the molecular $\mathbf{G}$ matrix can also be constructed approximately. This NESC variant, which is essentially as accurate as standard NESC, has been coined NESC with atomic unitary transformation (NESCau, i.e. X2Cau) [56]. Since the approximate $\mathbf{U}$ and $\mathbf{G}$ matrices in NESCau do not depend on molecular geometries, analytic calculations of nuclear gradients and Hessians are very efficient [56], and therefore can be used to investigate large molecules as is demonstrated in this study.

2.2. The local vibrational mode analysis

The central starting point is Wilson's theory of vibrational spectroscopy. In Equation (8), the Wilson equation of vibrational spectroscopy for a vibrating systems with N atoms is given [111–117]:

$$\mathbf{F}^x\tilde{\mathbf{L}} = \mathbf{M}\tilde{\mathbf{L}}\mathbf{\Lambda} \tag{8}$$

where $\mathbf{F}^x$ is the force constant matrix or Hessian matrix expressed in Cartesian coordinates x_i (i = 1, ⋯ $3N$). $\mathbf{M}$ is the mass matrix and matrix $\tilde{\mathbf{L}}$ collects the vibrational eigenvectors $\mathbf{l}_\mu$ in its columns ($\mu = 1, \ldots, N_{\mathrm{vib}}$). The number of vibrational modes N_{vib} equals $3N$ – N_{tr} with the translational and rotational modes N_{tr} being 5 for linear and 6 for non-linear molecules. $\mathbf{\Lambda}$ is a diagonal matrix with the eigenvalues λ_μ, which leads to the (harmonic) vibrational frequencies ω_μ according to $\lambda_\mu = 4\pi^2c^2\omega_\mu^2$. The tilde symbol indicates mass weighting. The normal mode eigenvectors and eigenvalues are obtained by diagonalising the force constant matrix $\mathbf{F}^x$ defined in Equation (8) according to $\tilde{\mathbf{L}}^\dagger\mathbf{F}^x\tilde{\mathbf{L}} = \mathbf{\Lambda}$ and $\tilde{\mathbf{L}}^\dagger\mathbf{M}\tilde{\mathbf{L}} = \mathbf{I}$.

One usually re-normalises the normal mode vectors $\tilde{\mathbf{l}}_\mu$ according to $\mathbf{L} = \tilde{\mathbf{L}}\,(\mathbf{M}^R)^{1/2}$, where the elements of the mass matrix $\mathbf{M}^R$ are given by $m_\mu^R = (\tilde{\mathbf{l}}_\mu^\dagger\tilde{\mathbf{l}}_\mu)^{-1}$ and represent the reduced mass of mode μ.

Without mass-weighting Equation (8) takes the form [111,112,116]

$$\mathbf{F}^x\mathbf{L} = \mathbf{M}\mathbf{L}\mathbf{\Lambda} \tag{9}$$

leading to the diagonal normal force constant matrix $\mathbf{K}$, and the reduced mass matrix $\mathbf{M}^R$ in normal coordinates $\mathbf{Q}$, respectively.

$$\mathbf{L}^\dagger\mathbf{F}^x\mathbf{L} = \mathbf{K} \tag{10}$$

$$\mathbf{L}^\dagger\mathbf{M}\mathbf{L} = \mathbf{M}^R \tag{11}$$

The dimension of matrices $\mathbf{K}$ and $\mathbf{M}^R$ is $N_{\mathrm{vib}} \times N_{\mathrm{vib}}$.

It is often more convenient to express the molecular geometry in terms of internal coordinates $\mathbf{q}$ rather than Cartesian coordinates $\mathbf{x}$. Doing so the Wilson equation adopts the following form [111]:

$$\mathbf{F}^q\mathbf{D} = \mathbf{G}^{-1}\mathbf{D}\mathbf{\Lambda} \tag{12}$$

where $\mathbf{D}$ collects the normal mode vectors $\mathbf{d}_\mu$ ($\mu = 1, \ldots, N_{\mathrm{vib}}$) column-wise, and the Wilson matrix $\mathbf{G}$, which is defined as

$$\mathbf{G} = \mathbf{B}\mathbf{M}^{-1}\mathbf{B}^\dagger \tag{13}$$

represents the kinetic energy in terms of internal coordinates. The elements of the $\mathbf{B}$ matrix in Equation (13) are defined by the partial derivatives of internal coordinates with regard to Cartesian coordinates. It is important to note that the $\mathbf{B}$ matrix plays a central role for the Wilson equation of spectroscopy, namely connecting different sets of coordinates (internal, symmetry, curvilinear, etc.) with the Cartesian coordinates [111]. Therefore, whenever a new set of coordinates is introduced, the first step is to derive the appropriate $\mathbf{B}$ matrix. This is an important point for deriving a new bond strength measure for

metal–ring interactions, as discussed below. Diagonalisation of Equation (12) leads to

$$\mathbf{D}^{\dagger}\mathbf{F}^{q}\mathbf{D} = \mathbf{K} \tag{14}$$

Equations (9) and (12) are connected by the following equations [111]:

$$\mathbf{F^q} = \mathbf{C}^{\dagger}\mathbf{F^x}\mathbf{C} \tag{15}$$

$$\mathbf{D} = \mathbf{BL} \tag{16}$$

Matrix **C** is the pseudoinverse of the **B** matrix defined by

$$\mathbf{C} = \mathbf{W}\mathbf{B}^{\dagger}\left(\mathbf{B}\,\mathbf{W}\,\mathbf{B}^{\dagger}\right)^{-1} \tag{17}$$

where **W** is an arbitrary nonsingular $3N \times 3N$ square matrix. At a stationary point (*i.e.*, the energy gradient is a zero-vector), the N_{tr} translational and rotational eigenvectors are decoupled from the N_{vib} vibrational eigenvectors, and therefore **W** does not affect the results [118]. For reasons of simplicity, one often uses $\mathbf{W} = \mathbf{I}_{3N}$ (usually for the geometry optimisation procedure in internal coordinates) or $\mathbf{W} = \mathbf{M}^{-1}$. Using the latter definition, which is more physically sound [119] this leads to

$$\mathbf{C} = \mathbf{M}^{-1}\mathbf{B}^{\dagger}\mathbf{G}^{-1} \tag{18}$$

and

$$\mathbf{BC} = \mathbf{I}_{N_{\text{vib}}} \tag{19}$$

However, it should be noted that $\mathbf{CB} \neq \mathbf{I}_{3N}$ since **B** is spanned in a N_{vib} -dimensional vibrational space.

While the solution of the Wilson equation, i.e. the transformation to normal coordinates **Q** leads to a diagonal normal force constant matrix **K** free from any electronic coupling, there is still mass-coupling which prevents the direct use of normal mode force constants as intrinsic bond strength measure, a fact which often has been overlooked. In 1998, Konkoli and Cremer [75,76,120–122] derived for the first time local vibrational modes directly from normal vibrational modes by solving the mass-decoupled Euler-Lagrange equations, i.e. by solving the local equivalent of the Wilson equation for vibrational spectroscopy. They developed the leading parameter principle [75,120] which states that for any internal, symmetry, curvilinear, etc. coordinate a local mode $\mathbf{a}_n$ can be defined. $\mathbf{a}_n$ is independent of all other internal coordinates used to describe the geometry of a molecule, which means that it is also independent of using redundant or non-redundant coordinate sets. The local mode vector $\mathbf{a}_n$ associated with the nth internal coordinate q_n is defined as [75,120]

$$\mathbf{a}_n = \frac{\mathbf{K}^{-1}\mathbf{d}_n^{\dagger}}{\mathbf{d}_n\mathbf{K}^{-1}\mathbf{d}_n^{\dagger}} \tag{20}$$

where the local mode $\mathbf{a}_n$ is expressed in terms of normal coordinates **Q** and $\mathbf{d}_n$ is the nth row vector of the **D** matrix defined in Equation (16).

$$\mathbf{d}_n = \mathbf{b}_n\mathbf{L} \tag{21}$$

Equation (20) reveals that only matrices **K** and **D** are needed to determine $\mathbf{a}_n$, i.e. once the normal analysis is completed, a following local mode analysis is straight forward [75,120].

To each local mode $\mathbf{a}_n$ local mode properties can be assigned. The *local mode force constant* k_n^a of mode n (superscript a denotes an adiabatically relaxed, i.e. local mode) is obtained via Equation (22):

$$k_n^a = \mathbf{a}_n^{\dagger}\mathbf{K}\mathbf{a}_n = (\mathbf{d}_n\mathbf{K}^{-1}\mathbf{d}_n^{\dagger})^{-1} \tag{22}$$

It is noteworthy that local mode force constants, contrary to normal mode force constants, have the advantage of being independent of the choice of the coordinates used to describe the molecule in question [75,76].

The *local mode mass* m_n^a of mode n is given by

$$m_n^a = 1/G_{n,n} = (\mathbf{b}_n\mathbf{M}^{-1}\mathbf{b}_n^{\dagger})^{-1} \tag{23}$$

where $G_{n,n}$ is the nth diagonal element of the Wilson **G** matrix. For a chemical bond A-B, Equation (23) leads to $M_AM_B/(M_A + M_B)$, which has the same form as the reduced mass of diatomic molecules.

Local mode force constant and mass are needed to determine the *local mode frequency* ω_n^a

$$(\omega_n^a)^2 = \frac{1}{4\pi^2c^2}k_n^aG_{nn} \tag{24}$$

Apart from these properties, it is straightforward to determine other local mode properties, such as infrared intensities [77].

In the following, we will derive a local mode stretching force constant for the An-ring interaction. One could think of calculating the local modes for all An-ring carbon interactions and averaging over the corresponding local mode force constants. A better way is to use only one interaction parameter describing the local stretching between the An atom and the centre M of the ring, as depicted in Figure 3 leading to a straight forward comparison of the strength of An-ring interaction in different An-sandwich complexes.

Similar to the stretching between two atoms [111], the **B**-matrix of the stretching between the An atom and the

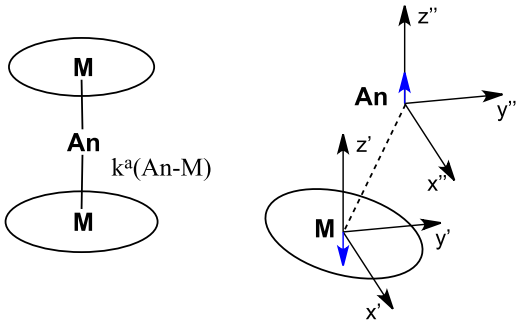

Figure 3. Definition of the local mode force constant k^a(An-M) describing the An-ring interaction, M denotes the ring centre.

geometrical centre of the ring defined by dummy atom M can be calculated via the unit vector $\mathbf{e}_{1,2} = \mathbf{r}_{1,2}/r_{1,2}$ from An to M,

$$\mathbf{s}_{An} = \mathbf{e}_{2,1} = -\mathbf{e}_{1,2} \tag{25}$$

$$\mathbf{s}_M = \mathbf{e}_{1,2} \tag{26}$$

and the three **B**-matrix elements $B_{i,x}$, $B_{i,y}$ and $B_{i,z}$ for each ring atom i are given by

$$\mathbf{s}_i = \frac{1}{N_j}\mathbf{s}_M \tag{27}$$

where N_j denotes the number of ring atoms.

In order to determine the position of M, the Cartesian coordinate system is rotated into the standard orientation with uniquely defined the standard x-, y- and z-axes, which is defined by the Cremer-Pople mean ring plane [123,124] of the ring atoms. As sketched in Figure 3, one can then uniquely define a projected stretching direction $\mathbf{e}'_{1,2} = \mathbf{r}_{1',2}/r_{1',2}$ along the normal vector direction $\overrightarrow{\mathbf{n}}$ of the ring's unique mean plane [123,124], and derive the force constant k^a(An-M) and related frequency ω^a(An-M).

The local mode analysis was complemented with the Natural Bond Orbital (NBO) analysis [105,125–127] to determine the 5f orbital occupation number of the An atom in each compound, in this way identifying which of the 5f orbitals are participating in bonding. In order to examine the covalent character of the An-C bonds we applied the *Cremer-Kraka Criterion* [128–130] for covalent bonding, which is based on the local energy density H(**r**)

$$\mathrm{H}(\mathbf{r}) = G(\mathbf{r}) + V(\mathbf{r}) \tag{28}$$

where $G(\mathbf{r})$ is kinetic energy density (positive, destabilising) and $V(\mathbf{r})$ is potential energy density (negative, stabilising). Taken at the bond critical point r_b of the electron density $\rho(\mathbf{r})$ [131] between two bonded atoms, $\mathrm{H}(r_b) < 0$ indicates a covalent bond, while $\mathrm{H}(r_b) > 0$ indicates an electrostatic interaction.

The set of 20 complexes $An(C_nH_n)_2$ (An : Th(IV), Pa(V), U(IV), Np(IV), Pu(IV); $C_nH_n = [C_5H_5]^-$, C_6H_6, $[C_7H_7]^+$, $[C_8H_8]^{2-}$) and as a reference $Fe(C_5H_5)_2$ were calculated at the NESCau/M06 level of theory [132] utilising the Jorge-triple zeta valence quality plus polarisation (Jorge-TZP-DKH) basis set for all metals and the double zeta (Jorge-DZP-DKH) for carbon and hydrogen atoms [133–136]. These basis sets have been reported as an efficient choice for relativistic calculations of actinide compounds, because of a balanced description of core and valence electrons [136,137]. The NESCau/M06 geometry optimisations and frequencies calculations, as well as the subsequent local mode analysis was carried out with the Cologne2020 program package [138]. For the NBO analysis, the NBO 6 program [139] was used, whereas the topological electron density analysis of $\rho(\mathbf{r})$ was carried out with the program AIMAll [140].

3. Results and discussion

3.1. Geometries and strength of the an-ring interaction

The optimised geometries of all complexes $An(C_nH_n)_2$ (An : Th, Pa, U, Np, Pu; $n = 5-8$) are of D_{nh} symmetry with a linear M-An-M arrangement, with one exception; the $An(C_6H_6)_2$ complexes adapt C_{2v} symmetry with a bent M-An-M arrangement (see Figure 2), in line with other studies [141–144]. All complexes were identified as minimum structures on the potential energy surface; i.e. no imaginary vibrational frequencies were encountered. Possible reasons for the bent structures are i) the competition between ligand repulsion and bond stabilisation, discussed in the literature as a common feature of actinide sandwich complexes [145,146], or ii) a Jahn-Teller or pseudo-Jahn Teller distortion [147,148], which so far has been mostly observed for 3d-metal sandwich compounds [149,150]. Work is in progress to further explore possible Jahn-Teller distortions in 5f-metal complexes in more detail.

The results of our relativistic calculations are presented in Table 1. The calculated distances between the metal and the centre of the ring (An-M) for $Th(C_8H_8)_2$, $U(C_8H_8)_2$ and $Np(C_8H_8)_2$ are 1.999, 1.930, 1.911 Å, respectively, in good agreement with the corresponding experimental values of 2.004, 1.926 and 1.909 Å [151,152]. The same holds for the Fe-M distance of $Fe(C_5H_5)_2$; the calculated distance is 1.644 Å and the experimental distance is 1.648 Å [153,154]. This confirms the validity of our chosen NESCau/M06 model chemistry.

Table 1. Summary of Geometric, and Vibrational Data for Complexes $An(C_nH_n)_2$.[a]

	q (An-M)	k^a (An-M)	ω^a (An-M)	R	$\Delta(R-q)$	k^a (An-C)	ω^a (An-C)	5f (An)	$\rho(r_b)$ (An-C)	$H(r_b)$ (An-C)	$\rho(r_c)$ (An-M)	$H(r_c)$ (An-M)
$Fe(C_5H_5)_2$	1.644	3.424	549.8	2.041	0.397	1.76	448.1		0.6264	−0.2321		
$(C_5H_5)_2$												
Th	2.429	2.854	388.2	2.707	0.278	1.013	318.8	0.01	0.3042	−0.0495	0.2207	0.0227
Pa	2.450	2.314	363.2	2.731	0.281	0.886	287.1	1.18	0.2666	0.0045	0.1917	0.0235
U	2.363	1.659	333.1	2.648	0.285	0.747	258.4	2.81	0.3178	−0.0222	0.2254	0.0227
Np	2.345	1.261	302.3	2.635	0.290	0.618	227.0	4.22	0.3259	−0.0251	0.2200	0.0240
Pu	2.335	2.024	350.3	2.626	0.291	0.827	267.3	4.96	0.2956	−0.0144	0.2254	0.0227
$(C_6H_6)_2$												
Th	2.253	2.361	385.7	2.607	0.354	1.003	297.7	0.00	0.3336	−0.0410	0.1464	0.0223
Pa	2.163	2.473	332.1	2.591	0.428	1.123	271.3	1.36	0.2174	−0.0104	0.1377	0.0345
U	2.310	1.576	338.7	2.539	0.229	0.775	242.4	2.63	0.2747	−0.0456	0.1599	0.0283
Np	2.257	1.075	369.7	2.512	0.255	0.922	211.4	3.78	0.2173	−0.0374	0.1613	0.0276
Pu	2.138	2.191	333.3	2.563	0.425	1.165	250.1	4.87	0.3064	−0.0269	0.1599	0.0283
$(C_7H_7)_2$												
Th	2.036	2.573	402.4	2.609	0.573	1.088	275.5	0.02	0.3381	−0.0493		
Pa	2.007	3.174	310.0	2.777	0.770	1.095	247.5	1.62	0.2474	−0.0021		
U	2.144	1.566	375.4	2.482	0.338	0.948	231.2	2.43	0.2917	−0.0314		
Np	2.096	1.179	321.9	2.601	0.505	0.857	211.4	4.03	0.2477	−0.0063		
Pu	2.130	1.833	318.7	2.674	0.544	0.917	223.4	4.82	0.2643	0.0019		
$(C_8H_8)_2$												
Th	1.999	3.548	412.6	2.651	0.652	1.145	266.1	0.00	0.3151	−0.0424		
Pa	1.981	2.442	363.8	2.686	0.705	0.890	209.9	1.73	0.2760	0.0026		
U	1.930	2.147	369.2	2.651	0.721	0.917	206.9	2.76	0.3232	−0.0041		
Np	1.911	1.288	334.3	2.616	0.705	0.752	179.6	4.19	0.2699	−0.0270		
Pu	1.987	1.650	320.3	2.710	0.723	0.771	211.3	5.79	0.2653	−0.0147		

[a] Calculated at NESCau/M06/Jorge-(T/D)ZP-DKH (T for An, D for C and H) level of theory. q metal–ring distances in Å; k^a(An-M) local stretching force constants of An-ring interactions in mDyn/Å; ω^a(An-M) local stretching frequency of An-ring interactions in cm^{-1}; R (An-C) bond length in Å; $\Delta(R-q)$ the difference between A-C bond length and A-M metal–ring length; k^a(An-C) the average of local stretching force constants of An-C bonds in mDyn/Å; ω^a(An-C) the average of local stretching frequency of An-C bond in cm^{-1}; 5f occupation numbers of An; $\rho(r_b)$ the average of density and $H(r_b)$ the average of energy density at bond critical point between An and each C-atom of the ring in e/$Å^3$ and Hartree/$Å^3$, respectively; $\rho(r_c)$ the density at the cage critical point in e/$Å^3$; $H(r_c)$ the energy density at the cage critical point in Hartree/$Å^3$.

The weakest metal–ring interactions are observed for the Np-complexes with an average k^a(An-M) value of 1.200 mDyn/Å, and the strongest interactions for the Th- and Pa-complexes, with average k^a(An-M) values of 2.834 and 2.600 mDyn/Å, respectively. In comparison, the ferrocene complex has a local mode force constant k^a(An-M) of 3.424 mDyn/Å. Figure 4 shows the relationship between the local force constant k^a(An-M) and the An-M distance. The $An(C_5H_5)_2$ complexes have the longest An-M distances, while $An(C_8H_8)_2$ the shortest. The local force constants k^a range from 1.075 mDyn/Åfor $Np(C_6H_6)_2$, (i.e. weakest interaction) to 3.548 mDyn/Åfor $Th(C_8H_8)_2$, (strongest interaction, even stronger than the Fe-M interaction with 3.424 mDyn/Å). This shows that the metal centre plays a key role with regard to the strength of the An-M interaction.

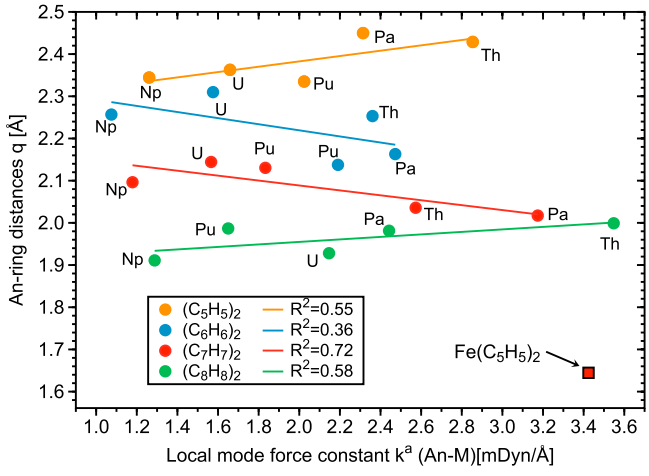

Figure 4. An-M distance *q* vs. local stretching force constant k^a(An-M). Calculated at the NESCau/M06/Jorge-(T/D)ZP-DKH (T for An, D for C and H) level of theory.

Although there is no overall significant correlation between distance and strength, we can see some trends. For the sandwich complexes with 6-membered (6MR) and 7-membered (7MR) rings we find a Badger-type [155] relationship, i.e. for each of the series a shorter distance relates to a stronger interaction. However, for the sandwich complexes with five-membered (5MR) rings, (longest An-M distances) and 8-membered (8MR) rings, (shortest An-M distances), we find an inverse Badger relationship, i.e. within each of this series the longer An-M distance is paired with larger local force constant. In both cases, the ring is negatively charged leading to electrostatic repulsion between ring and metal centre. This is in line with previous studies where we observed increased bond weakening with decreasing bond length for chemical bonds between two electronegative atoms (e.g. NF)

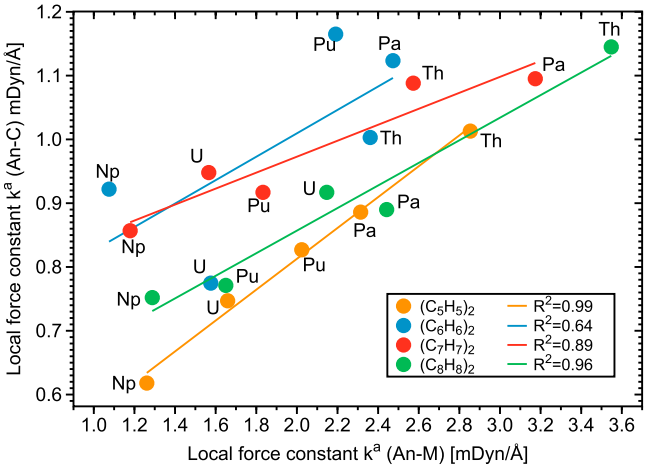

Figure 5. Relationship between the local force constants k^a(An-C) averaged over all ring An-C bonds for each ring and the local stretching force constants k^a(An-M) for the metal ring centre interaction. Calculated at the NESCau/M06/Jorge-(T/D)ZP-DKH (T for An, D for C and H) level of theory.

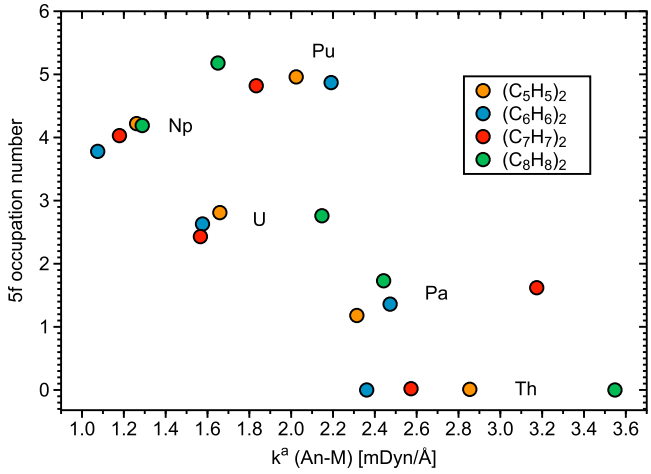

Figure 6. 5f occupation numbers of the An atoms vs local stretching force constants k^a(An-M). Calculated at the NESCau/M06/Jorge-(T/D)ZP-DKH (T for An, D for C and H) level of theory.

caused by increasing electrostatic repulsion, which overrules the Badger rule [83,156].

Figure 5 correlates the local mode force constants k^a(An-C) averaged over all ring An-C bonds for each ring and the local stretching force constant k^a(An-M) for the metal–ring centre interaction. There is a significant correlation between both local force constants for the 5MR, 7MR and 8 MR sandwich compounds. However, Figure 5 clearly reveals that the former are smaller, i.e. the strength of the interaction between the metal and the ring ligands is underestimated when using the average interaction between the metal and the individual carbon atoms of the ring as bond strength measure. This is also reflected by the local vibrational frequencies ω^a values collected in Table 1. In the case of the bent 6MR sandwich complexes the correlation between the two force constants falls short, confirming that only the local k^a(An-M) force constants are suited as intrinsic bond strength measure, applicable to complexes with higher and lower symmetry.

3.2. NBO analysis and 5f occupation

Actinides are characterised by gradually filling the 5f-electron shell. The level of localisation and participation of the actinide 5f valence orbitals in covalent bonds across the actinide series is still an ongoing debate [157,158]. The 5f orbitals of actinides can be localised like 4f orbitals in the lanthanide series, or delocalised like d orbitals in transition metals. Also, relativistic effects can move the 5f and 6d orbital energies closer together, allowing both orbitals to participate in chemical bonding [159].

In order to describe the role of 5f electrons in An-ring bonding, the 5f orbital occupation number of the An atom of each compound investigated in this work was calculated via an NBO analysis and compared with the corresponding local stretching force constant k^a(An-M). In Table 1 all 5f occupation numbers are collected. In Figure 6, the 5f occupation numbers are compared with the local stretching force constants k^a(An-M). An isolated Th atom with the electron configuration of $[Xe]6d^27s^2$ has no 5 f occupation. This is reflected by the close to zero values in Table 1 found for all Th sandwich complexes, independent of the type and size of the ring. However, as depicted in Figure 6 the local k^a(An-M) force constants vary from 2.361 mDyn/Å(6MR) to 3.584 mDyn/Å(8MR), showing a clear variation in metal–ring bonding. This indicates that 5f molecular orbitals do not participate in the Th-ring interaction, in line with the finding that Th tends to resemble d-block transition metals [160,161]. The 5f occupation numbers of the Pa complexes are in the range of 1.18 e (5MR)–1.73 e (8MR), being smaller than the 5f occupation number in the isolated Pa atom ($[Xe]5f^26d^17s^2$). However, there is no direct correlation with the local stretching force constants k^a(Pa-M), i.e. the interaction is not dominated by 5f electron participation.

The same holds for the 5f occupation numbers of the U-complexes ranging from 2.43 e (7MR) –2.81 e (5MR) which are smaller than that of the isolated U atom ($[Xe]5f^36d^17s^2$.) Again, there no direct correlation between 5f delocalisation and bond strength, the largest k^a(U-M) value of 2.417 mDyn/Å is found for the 8MR while the smallest 5f occupation number of 2.43 e, i.e.

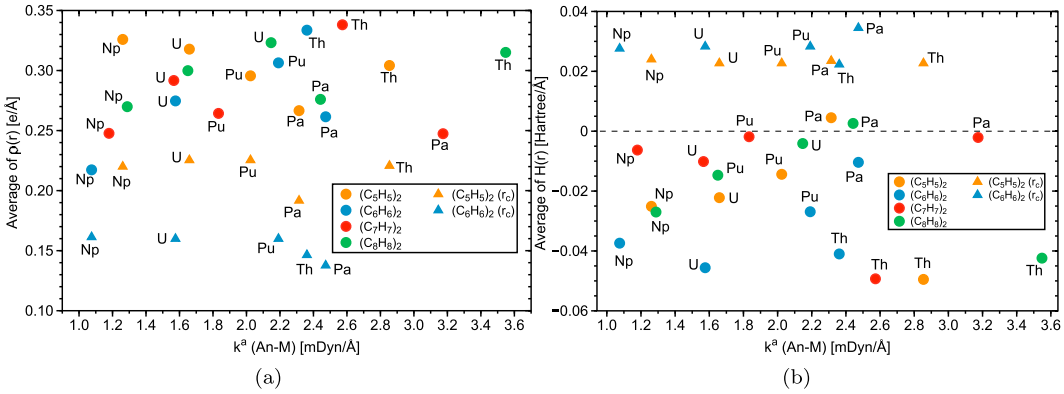

Figure 7. (a) Average electron density $\rho(r_b)$ and $\rho(r_c)$ vs k^a(An-M); (b) $H(r_b)$ and $H(r_c)$ vs k^a (An-M). Calculated at the NESCau/M06/Jorge-(T/D)ZP-DKH (T for An, D for C and H) level of theory.

largest delocalisation is found for the 7MR. The 5f occupation numbers for the Np-complexes are close to the configuration of the isolated Np atom ($[Xe]5f^46d^17s^2$). It is interesting to note that in the case of the 5MR and 8MR the 5f occupation number is larger than 4 (4.22 e, 5MR and 4.19 e, 8MR) indicating a delocalisation of charge from the negatively charged ring into the 5f orbitals, which correlates with the higher k^a(An-M) values of 1.261 mDyn/Å, 5MR and 1.288 mDyn/Å, 8MR. However, overall the Np complexes have the weakest metal–ring interaction compared to other An-complexes, in line with arguments that the 5f electrons in Np are more localised and less prone to metal–ring interactions [160,162]. The 5f occupation numbers of the Pu-complexes are in a range of 4.82 e (7MR)–5.79 e (8MR) which are again smaller than the 5f occupation number in the isolated Pu atom ($[Xe]5f^66d^07s^2$). But also in this case there is no direct correlation between 5f electron occupation and the strength of the metal–ring interaction.

3.3. Electron and energy density distribution

The local mode and the NBO analyses were complemented with the topological analysis of the electron density $\rho(\mathbf{r})$ focusing on the characterisation of the An-C bonds. Table 1 collects the electron density $\rho(r_b)$ at the An-C bond critical point r_b averaged over all An-C ring bonds for each ring and the corresponding energy density $H(r_b)$. For 5MR and 6MR complexes in addition to bond critical points r_b also cage critical points r_c [131] were found. The corresponding electron density $\rho(r_c)$ and energy density $H(r_c)$ at the cage critical point are also included in Table 1. In Figure 7(a), $\rho(r_b)$ and $\rho(r_c)$ values are compared with the local mode force constants k^a(An-M), whereas Figure 7(b) relates energy density $H(r_b)$ and $H(r_c)$ with the local mode force constants k^a(An-M).

As discussed above, the covalent character of a chemical bond is reflected by a negative value of $H(r_b)$, while a positive energy density $H(r_b)$ corresponds to a chemical bond with dominant electrostatic character [129,130,163]. The energy density $H(r_b)$ of the Th-complexes is between −0.0410 and −0.0495 Hartree/Å^3 indicating the covalent character of the Th-C ring bonds, which correlates with larger local mode force constants k^a(An-M), see Table 1 and Figure 7(b). $Pa(C_5H_5)_2$, $Pa(C_7H_7)_2$ and $Pa(C_8H_8)_2$ complexes have $H(r_b)$ values from −0.0021 to 0.0045 Hartree/Å^3, showing a mixture of the electrostatic and the covalent bonding between metal and ring atoms. The $Pa(C_6H_6)_2$ complex which has a bent geometry contrary to the linear M–Pa–M arrangement of the other Pa sandwich complexes, has an $H(r_b)$ value of −0.0304 Hartree/Å^3, revealing larger covalent character of the Pa–C bonds. This can be explained by the larger overlap between the π orbitals of benzene with the 6d and 5f orbitals of the metal in the bent geometry, leading to stronger electron donation from the ring and to more covalent bonding character. The same effect is true for the bent $U(C_6H_6)_2$, $Np(C_6H_6)_2$ and $Pu(C_6H_6)_2$ complexes. The only exception is the bent $Th(C_6H_6)_2$ complex, showing less covalent character than the other Th complexes. In this case, the 5f orbitals are empty, and the bent structure does not necessarily lead to a stronger electron donation from the ring to the metal atom. Overall, as depicted in Figure 7(a,b), there is no direct correlation between An-C bond critical point properties and the intrinsic strength of the An-ring interaction represented via the local mode force constants k^a(An-M).

4. Conclusion

This work provides a detailed analysis of $An(C_nH_n)_2$ (An: Th, Pa, U, Np, Pu; $n = 5–8$) sandwich complexes combining the NESCau approach and the local vibrational mode analysis. We could shed new light on

the An-carbon bonding and the An-ring interactions in these f-block sandwich complexes including the following highlights:

- Our study shows that NESCau is an easily applicable method providing a solid fundament for the calculation of compounds with superheavy elements. Building upon the locality of relativistic effects, NESCau makes NESC calculations dozens to hundreds of times faster without losing accuracy [56].
- $An(C_nH_n)_2$ complexes with smaller ring are characte rised by longer An-ring distances than complexes with larger rings. However, the strength of the An-ring interaction does not correlate with ring size and/or metal–ring distance; it is determined by the character of the metal centre. The weakest An-ring interactions were observed for $Np(C_nH_n)_2$ while the strongest for $Th(C_nH_n)_2$ complexes.
- Calculated 5f occupation numbers are in line with the expected An oxidation states. They increase across the actinide series denoting a successive increase of the electron localisation on the An centre with increasing atomic number. As reflected by the corresponding local mode force constants, delocalisation of the 5f-orbitals leads to a weakening of the An-ring interaction. Th complexes with a 5f occupation number close to zero have the strongest An-ring interactions. This clearly shows that in these compounds 5f orbitals do not play a role for the metal–ring interactions.
- According to the Cremer-Kraka criterion strongest covalent An-C bonds were observed in Th-complexes, followed by U and Np complexes, while Pu and in particular Pa complexes showed a mixture of covalent bonding and electrostatic interactions.

By rationalising the intrinsic strength of An-C bonding and An-ring interactions and their interplay in a series of 20 An sandwich complexes $An(C_nH_n)_2$, this work provides valuable information for the fine-tuning and future synthesis of An sandwich compounds. We also hope to encourage by our study the use of NESCau for the investigation of large systems with heavy metal and superheavy metal atoms.

Acknowledgements

The authors thank SMU for providing excellent computational resources.

Disclosure statement

No potential conflict of interest was reported by the author(s).

Funding

This work was finally supported by the National Science Foundation [Grant Number CHE 1464906]. At Xi'an, this work was supported by the Double First-Class University Construction Project of Northwest University.

ORCID

Małgorzata Z. Makoś http://orcid.org/0000-0002-6015-5608
Marek Freindorf http://orcid.org/0000-0001-5285-5455
Elfi Kraka http://orcid.org/0000-0002-9658-5626

References

[1] T.J. Kealy and P.L. Pauson, Nature **168** (4285), 1039–1040 (1951).
[2] P.J. Chirik, Organometallics **29**, 1500–1517 (2010).
[3] A. Streitwieser and U. Mueller-Westerhoff, J. Am. Chem. Soc. **90** (26), 7364–7364 (1968).
[4] R.G. Hayes and N. Edelstein, J. Am. Chem. Soc. **94** (25), 8688–8691 (1972).
[5] K.D. Warren, Inorg. Chem. **13** (6), 1317–1324 (1974).
[6] A. Chandrasekar, M. Joshi, and T.K. Ghanty, J. Chem. Sci. **131** (12), 122 (2019).
[7] H. Braunschweig, M.A. Celik, K. Dück, F. Hupp, and I. Krummenacher, Chem. Eur. J. **21** (26), 9339–9342 (2015).
[8] S.D. Jiang, S.S. Liu, L.N. Zhou, B.W. Wang, Z.M. Wang, and S. Gao, Inorg. Chem. **51** (5), 3079–3087 (2012).
[9] J.T. Boronski, L.R. Doyle, J.A. Seed, A.J. Wooles, and S.T. Liddle, Angew. Chem **59** (1), 295–299 (2019).
[10] N. Kaltsoyannis, Chem. Eur. J. **24** (12), 2815–2825 (2017).
[11] F.T. Edelmann, J.H. Farnaby, F. Jaroschik, and B. Wilson, Coord. Chem. Rev. **398**, 113005 (2019).
[12] G. Feng, M. Zhang, D. Shao, X. Wang, S. Wang, L. Maron, and C. Zhu, Nature Chem. **11** (3), 248–253 (2019).
[13] M.A. Boreen, T.D. Lohrey, G. Rao, R.D. Britt, L. Maron, and J. Arnold, J. Am. Chem. Soc. **141** (13), 5144–5148 (2019).
[14] N. Tsoureas, A. Mansikkamäki, and R.A. Layfield, Chem. Comm. **56** (6), 944–947 (2020).
[15] O. Walter, Chem. Eur. J. **25**, 2927–2934 (2018).
[16] P.L. Arnold, M.S. Dutkiewicz, and O. Walter, Chem. Rev. **117** (17), 11460–11475 (2017).
[17] G.M. Rand, P.G. Wells, and L.S. McCarty, in *Fundamentals of Aquatic Toxicology*, edited by G. M. Rand (Taylor and Francis, Washington, DC, 1995), pp. 3–66.
[18] J.H. Duffus, Pure Appl. Chem. **74** (5), 793–807 (2002).
[19] J. Desclaux, At. Data Nucl. Data Tables **12**, 311–406 (1973).
[20] I.P. Grant, *Relativistic Quantum Theory of Atoms and Molecules, Theory and Computation* (Springer, New York, 2007).
[21] P. Pyykkö, Chem. Rev. **88**, 563–594 (1988).
[22] P. Pyykkö, Ann. Rev. Phys. Chem. **63**, 45–64 (2012).
[23] K.G. Dyall, J. Chem. Phys. **106**, 9618–9626 (1997).
[24] K.G. Dyall, J. Com. Chem. **23** (8), 786–793 (2002).
[25] M. Filatov and D. Cremer, Chem. Phys. Lett. **370** (5–6), 647–653 (2003).

[26] D. Cremer, W. Zou, and M. Filatov, WIREs Comput. Mol. Sci. **4** (5), 436–467 (2014).
[27] W. Zou, M. Filatov, and D. Cremer, J. Chem. Phys. **134** (24), 244117 (2011).
[28] L. Cheng and J. Gauss, J. Chem. Phys. **135**, 084114 (2011).
[29] W. Zou, M. Filatov, and D. Cremer, J. Chem. Phys. **142** (21), 214106 (2015).
[30] Y.J. Franzke, N. Middendorf and F. Weigend, J. Chem. Phys. **148** (10), 104110 (2018).
[31] L. Cheng and J. Gauss, J. Chem. Phys. **135**, 244104 (2011).
[32] W. Zou, M. Filatov, and D. Cremer, J. Chem. Theory Comput. **8** (8), 2617–2629 (2012).
[33] V.A. Nasluzov and N. Rösch, Chem. Phys. **210** (3), 413–425 (1996).
[34] A.V. Matveev, V.A. Nasluzov, and N. Rösch, Int. J. Quantum Chem. **107** (15), 3236–3249 (2007).
[35] A. Wolf and M. Reiher, J. Chem. Phys. **124** (6), 2037 (2006).
[36] M. Reiher and A. Wolf, J. Chem. Phys. **121** (22), 10945–10956 (2004).
[37] C. Van Wüllen, Chem. Phys. **311** (1–2), 105–112 (2005).
[38] C. Van Wüllen, J. Chem. Phys. **120** (16), 7307–7313 (2004).
[39] M. Barysz, Ł. Mentel, and J. Leszczyński, J. Chem. Phys. **130** (16), 164114 (2009).
[40] M. Barysz, A.J. Sadlej, and J.G. Snijders, Int. J. Quantum Chem. **65** (3), 225–239 (1997).
[41] Y. Nakajima, J. Seino, and H. Nakai, J. Chem. Theory Comput. **12** (5), 2181–2190 (2016).
[42] J. Tao, J. P. Perdew, V.N. Staroverov, and G.E. Scuseria, Phys. Rev. Lett. **91** (146401), 1–14 (2003).
[43] R.P. Feynman, *Quantum Electrodynamics (New Ed.)* (Westview Press, New York, 1998).
[44] C. Cohen-Tannoudji, J. Dupont-Roc, and G. Grynberg, *Photons and Atoms: Introduction to Quantum Electrodynamics* (Wiley-Interscience, Canada, 1997).
[45] P.A.M. Dirac, Proc. R. Soc. (London) **A123** (792), 714–733 (1929).
[46] P.A. Dirac, Rev. Mod. Phys. **21**, 392 (1949).
[47] M. Douglas and N.M. Kroll, Ann. Phys. (NY) **82**, 89–155 (1974).
[48] B.A. Hess, Phys. Rev. A **32** (2), 756–763 (1985).
[49] E. van Lenthe, J. Snijders, and E. Baerends, J. Chem. Phys. **105**, 6505–6516 (1996).
[50] T. Nakajima and K. Hirao, J. Chem. Phys. **113**, 7786–7789 (2000).
[51] C. van Wuellen, J. Chem. Phys. **120**, 7307–7313 (2003).
[52] M. Reiher and A. Wolf, J. Chem. Phys. **121**, 10945–10956 (2004).
[53] E. van Lenthe, E.J. Baerends, and J.G. Snijders, J. Chem. Phys. **101**, 9783–9792 (1994).
[54] C. van Wuellen, J. Chem. Phys. **109**, 392–399 (1998).
[55] M. Filatov, J. Chem. Phys. **125** (10), 107101 (2006).
[56] W. Zou, G. Guo, B. Suo, and W. Liu, J. Chem. Theory Comput. **16**, 1541–1554 (2020).
[57] W. Liu and D. Peng, J. Chem. Phys. **131** (3), 031104 (2009).
[58] D. Peng and M. Reiher, Theor. Chem. Acc. **131** (1), 1018 (2012).
[59] D. Peng, W. Liu, Y. Xiao, and L. Cheng, J. Chem. Phys. **127**, 104106 (2007).
[60] W. Liu and D. Peng, J. Chem. Phys. **131**, 031104 (2009).
[61] M. Iliaš and T. Saue, J. Chem. Phys. **126**, 064102 (2007).
[62] M. Filatov, W. Zou, and D. Cremer, J. Phys. Chem. A **116** (13), 3481–3486 (2012).
[63] M. Filatov, W. Zou, and D. Cremer, J. Chem. Theory Comput. **8** (3), 875–882 (2012).
[64] M. Filatov, W. Zou, and D. Cremer, J. Chem. Phys. **137** (5), 054113 (2012).
[65] W. Zou, M. Filatov, and D. Cremer, J. Chem. Phys. **137** (8), 084108 (2012).
[66] M. Filatov, W. Zou and D. Cremerv Int. J. Quant. Chem. **114** (15), 993–1005 (2013).
[67] T. Yoshizawa, W. Zou, and D. Cremer, J. Chem. Phys. **145** (18), 184104 (2016).
[68] T. Yoshizawa, M. Filatov, D. Cremer, and W. Zou, Mol. Phys. **117** (9–12), 1164–1171 (2019).
[69] T. Yoshizawa, W. Zou, and D. Cremer, J. Chem. Phys. **146** (13), 134109 (2017).
[70] M. Barysz, L. Mentel, and J. Leszczynski, J. Chem. Phys. **130**, 164114 (2009).
[71] T. Oyama, Y. Ikabata, J. Seino, and H. Nakai, Chem. Phys. Lett. **680**, 37–43 (2017).
[72] M. Barysz, A.J. Sadlej, and J.G. Snijders, Int. J. Quantum Chem. **65**, 225–239 (1997).
[73] D. Peng and M. Reiher, Theor. Chem. Acc. **131**, 1081 (2012).
[74] Y.J. Franzke, N. Middendorf, and F. Weigend, J. Chem. Phys. **148**, 104110 (2018).
[75] Z. Konkoli and D. Cremer, Int. J. Quant. Chem. **67** (1), 1–9 (1998).
[76] D. Cremer, J.A. Larsson, and E. Kraka, in *Theoretical and Computational Chemistry*, edited by C. Parkanyi (Elsevier, Amsterdam, 1998), pp. 259–327.
[77] W. Zou and D. Cremer, Theor. Chem. Acc. **133**, 1451–1466 (2014).
[78] E. Kraka and D. Cremer, Int. J. Quantum Chem. **119** (6), e25849 (2019).
[79] E. Kraka and D. Cremer, ChemPhysChem **10** (4), 686–698 (2009).
[80] E. Kraka, J.A. Larsson, and D. Cremer, in *Computational Spectroscopy*, edited by J. Grunenberg (Wiley, New York, 2010), pp. 105–149.
[81] R. Kalescky, E. Kraka, and D. Cremer, J. Phys. Chem. A **117** (36), 8981–8995 (2013).
[82] W. Zou and D. Cremer, Chem. Eur. J. **22**, 4087–4097 (2016).
[83] E. Kraka, D. Setiawan, and D. Cremer, J. Comp. Chem. **37** (1), 130–142 (2015).
[84] D. Setiawan, D. Sethio, D. Cremer, and E. Kraka, Phys. Chem. Chem. Phys. **20** (37), 23913–23927 (2018).
[85] M.Z. Makoś, M. Freindorf, D. Sethio, and E. Kraka, Theor. Chem. Acc **138** (6), 76 (2019).
[86] D. Setiawan, E. Kraka, and D. Cremer, Chem. Phys. Lett. **614**, 136–142 (2014).
[87] D. Setiawan, E. Kraka, and D. Cremer, J. Phys. Chem. A **119** (9), 1642–1656 (2014).
[88] D. Setiawan, E. Kraka, and D. Cremer, J. Phys. Chem. A **119** (36), 9541–9556 (2015).
[89] D. Setiawan and D. Cremer, Chem. Phys. Lett. **662**, 182–187 (2016).

[90] V. Oliveira, E. Kraka, and D. Cremer, Phys. Chem. Chem. Phys. **18** (48), 33031–33046 (2016).
[91] V. Oliveira, E. Kraka, and D. Cremer, Inorg. Chem. **56** (1), 488–502 (2016).
[92] Y. Tao, W. Zou, J. Jia, W. Li, and D. Cremer, J. Chem. Theory Comput. **13** (1), 55–76 (2016).
[93] V. Oliveira and D. Cremer, Chem. Phys. Lett. **681**, 56–63 (2017).
[94] V. Oliveira, D. Cremer, and E. Kraka, J. Phys. Chem. A **121** (36), 6845–6862 (2017).
[95] V. Oliveira and E. Kraka, J. Phys. Chem. A **121** (49), 9544–9556 (2017).
[96] D. Sethio, V. Oliveira, and E. Kraka, Molecules **23** (11), 2763 (2018).
[97] S. Yannacone, V. Oliveira, N. Verma, and E. Kraka, Inorgan. **7** (4), 47 (2019).
[98] D. Sethio, L.M.L. Daku, H. Hagemann, and E. Kraka, Chem. Phys. Chem. **20** (15), 1967–1977 (2019).
[99] M. Freindorf, Y. Tao, D. Sethio, D. Cremer, and E. Kraka, Mol. Phys. **117** (9–12), 1172–1192 (2019).
[100] S. Lyu, N. Beiranvand, M. Freindorf, and E. Kraka, J. Phys. Chem. A **123**, 7087–7103 (2019).
[101] V.P. Oliveira, B.L. Marcial, F.B.C. Machado, and E. Kraka, Materials **13**, 55 (2020).
[102] W. Zou, Y. Tao, M. Freindorf, D. Cremer, and E. Kraka, Chem. Phys. Lett. **478**, 137337 (2020).
[103] Y. Tao, W. Zou, D. Sethio, N. Verma, Y. Qiu, C. Tian, D. Cremer, and E. Kraka, J. Chem. Theory Comput **15** (3), 1761–1776 (2019).
[104] Y. Tao, Y. Qiu, W. Zou, S. Nanayakkara, S. Yannacone, and E. Kraka, Molecules **25**, 1589 (2020).
[105] F. Weinhold, C. Landis, and E. Glendening, Int. Rev. Phys. Chem. **35** (3), 399–440 (2016).
[106] W. Zou, M. Filatov, and D. Cremer, Theor. Chem. Acc. **130** (4–6), 633–644 (2011).
[107] M. Filatov, W. Zou, and D. Cremer, J. Chem. Phys. **139** (1), 014106 (2013).
[108] D. Cremer, E. Kraka, and M. Filatov, ChemPhysChem **9** (17), 2510–2521 (2008).
[109] W. Zou, M. Filatov, D. Atwood, and D. Cremer, Inorg. Chem. **52** (5), 2497–2504 (2013).
[110] W. Liu, Phys. Rep. **537**, 59–89 (2014).
[111] E.B. Wilson, J.C. Decius, and P.C. Cross, *Molecular Vibrations* (McGraw-Hill, New York, 1955).
[112] L.A. Woodward, *Introduction to the Theory of Molecular Vibrations and Vibrational Spectroscopy* (Oxford University Press, Oxford, 1972).
[113] G. Herzberg, *Molecular Spectra and Molecular Structure*, I, 2nd Ed. (Reitell Press, New York, 2008).
[114] G. Herzberg, *Molecular Spectra and Molecular Structure. Volume II: Infrared and Raman Spectra of Polyatomic Molecules* (Krieger Publishing Co, New York, 1991).
[115] G. Herzberg and K.P. Huber, *Molecular Spectra and Molecular Structure* Constants of Diatomic Molecules, Vol. IV (Van Nostrand, Reinhold, New York, 1979).
[116] S. Califano, *Vibrational States* (Wiley, New York, 1976).
[117] R.J. Meier, Vib. Spectros. **43**, 26–37 (2007).
[118] W. Zou, R. Kalescky, E. Kraka, and D. Cremer, J. Chem. Phys. **137** (8), 084114 (2012).
[119] W. Zou, R. Kalescky, E. Kraka, and D. Cremer, J. Mol. Model. **19** (7), 2865–2877 (2012).
[120] Z. Konkoli, J.A. Larsson, and D. Cremer, Int. J. Quant. Chem. **67** (1), 11–27 (1998).
[121] Z. Konkoli and D. Cremer, Int. J. Quant. Chem. **67** (1), 29–40 (1998).
[122] Z. Konkoli, J.A. Larsson, and D. Cremer, Int. J. Quant. Chem. **67** (1), 41–55 (1998).
[123] W. Koch, G. Frenking, J. Gauss, D. Cremer, A. Sawaryn, and P. Schleyer, J. Am. Chem. Soc. **108** (19), 5732–5737 (1986).
[124] D. Cremer and J.A. Pople, J. Am. Chem. Soc. **97**, 1354–1358 (1975).
[125] F. Weinhold and C.R. Landis, Chem. Educ. Res. Pract. **2** (2), 91–104 (2001).
[126] A.E. Reed, L.A. Curtiss, and F. Weinhold, Chem. Rev. **88**, 899–926 (1988).
[127] J.P. Foster and F. Weinhold, J. Am. Chem. Soc. **102** (24), 7211–7218 (1980).
[128] D. Cremer and E. Kraka, Angew. Chem. Int. Ed. **23** (8), 627–628 (1984).
[129] D. Cremer and E. Kraka, Croatica Chem. Acta **57**, 1259–1281 (1984).
[130] E. Kraka and D. Cremer, in *Theoretical Models of Chemical Bonding. The Concept of the Chemical Bond*, edited by Z.B. Maksic, Vol. 2 (Springer Verlag, Heidelberg, 1990), p. 453.
[131] R.F.W. Bader, *Atoms in Molecules: A Quantum Theory* International series of monographs on chemistry (Oxford University Press, USA, 1990).
[132] Y. Zhao and D.G. Truhlar, Theor. Chem. Acc. **120** (1), 215–241 (2008).
[133] F.E. Jorge and A.B.F. da Silva, J. Chem. Phys. **104** (16), 6278–6285 (1996).
[134] E.V.R. de Castro and F.E. Jorge, J. Chem. Phys. **108** (13), 5225–5229 (1998).
[135] F.E. Jorge, A.C. Neto, G.G. Camiletti, and S.F. Machado, J. Chem. Phys. **130** (6), 064108 (2009).
[136] A. de Oliveira, C. Campos, F. Jorge, I. Ferreira, and P. Fantin, Comput. Theor. Chem. **1135**, 28–33 (2018).
[137] L.S.C. Martins, F.E. Jorge, M.L. Franco, and I.B. Ferreira, J. Chem. Phys. **145** (24), 244113 (2016).
[138] E. Kraka, W. Zou, M. Filatov, J. Gräfenstein, D. Izotov, J. Gauss, Y. He, A. Wu, Z. Konkoli, V. Polo, L. Olsson, Z. He, and D. Cremer, *LModeA* 2020, see http://www.smu.edu/catco.
[139] F. Weinhold and C.R. Landis, *Valency and Bonding: A Natural Bond Orbital Donor-acceptor Perspective* (Cambridge University Press, Cambridge, U.K., 2003). Theoretical Chemistry Institute, University of Wisconsin, Madison.
[140] T.A. Keith, *AIMAll Version 17.11.14* 2017, K Gristmill Software, Overland Park KS, USA..
[141] A. Kerridge, Dalton Trans. **42** (46), 16428 (2013).
[142] A. Kerridge, RSC. Adv. **4** (24), 12078–12086 (2014).
[143] M. Dolg and O. Mooßen, J. Organomet. Chem. **794**, 17–22 (2015).
[144] R.B. King, Appl. Organomet. Chem. **17** (6–7), 393–397 (2003).
[145] J. Zhou, J.L. Sonnenberg, and H.B. Schlegel, Inorg. Chem. **49**, 6545–6551 (2010).
[146] J. Berthet, P. Thuery, and M. Ephritikhine, Organometal lics **27**, 1664–1666 (2008).

[147] S.X. Hu, J.K. Gibson, W.L. Li, M.J.V. Stipdonk, J. Martens, G. Berden, B. Redlich, J. Oomens, and J. Li, Chem. Commun. **52**, 12761–12764 (2016).
[148] I.B. Bersuker, *The Jahn Teller Effect* (Cambridge University Press, London, 2010).
[149] L. Ma, J. Koka, and A.J. Stace, J. Phys. Chem. A **118**, 10730–10737 (2014).
[150] R.J. Deeth and M.A. Hitchman, Inorg. Chem. **25**, 122–1233 (1986).
[151] A. Avdeef, K.N. Raymond, K.O. Hodgson, and A. Zalkin, Inorg. Chem. **11** (5), 1083–1088 (1972).
[152] D.J.A.D. Ridder, J. Rebizant, C. Apostolidis, B. Kanellakopulos, and E. Dornberger, Acta Cryst. **52** (3), 597–600 (1996).
[153] K. Pierloot, B.J. Persson, and B.O. Roos, J. Phys. Chem. **99** (11), 3465–3472 (1995).
[154] C. Park and J. Almlöf, J. Chem. Phys. **95** (3), 1829–1833 (1991).
[155] R.M. Badger, J. Chem. Phys. **2** (3), 128–131 (1934).
[156] E. Kraka and D. Cremer, Rev. Proc. Quim. **11**, 39–42 (2012).
[157] T. Vitova, I. Pidchenko, D. Fellhauer, P.S. Bagus, Y. Joly, T. Pruessmann, S. Bahl, E. Gonzalez-Robles, J. Rothe, M. Altmaier, M.A. Denecke, and H. Geckeis, Nature Commun. **8** (1), 16053 (2017).
[158] D.L. Clark, S.S. Hecker, G.D. Jarvinen, and M.P. Neu, in *The Chemistry of the Actinide and Transactinide Elements*, edited by Lester R. Morss, Norman M. Edelstein, Jean Fuger and Joseph J. Katz (Springer, Netherlands, 2006), pp. 813–1210..
[159] R.B. King, Inorg. Chem **31**, 1978–1980 (1992).
[160] K.T. Moore and G. van der Laan, Rev. Mod. Phys. **81**, 235–298 (2009).
[161] M.S. Wickleder, B. Fourest, and P.K. Dorhout, in *The Chemistry of the Actinide and Transactinide Elements*, edited by Lester R. Morss, Norman M. Edelstein, Jean Fuger and Joseph J. Katz (Springer, Netherlands, 2006), p. 58.
[162] Z. Yoshida, S.G. Johnson, T. Kimura, and J.R. Krsul, in *The Chemistry of the Actinide and Transactinide Elements*, edited by Lester R. Morss, Norman M. Edelstein, Jean Fuger and Joseph J. Katz (Springer, Netherlands, 2006), pp. 699–780.
[163] D. Cremer and E. Kraka, J. Am. Chem. Soc. **107** (13), 3811–3819 (1985).